



# Fast and Highly Efficient Adsorption Removal of Toxic Pb(II) by a Reusable Porous Semi-IPN Hydrogel Based on Alginate and Poly(Vinyl Alcohol)

Wenbo Wang<sup>1,2\*</sup>, Xiangyu Liu<sup>1</sup>, Xue Wang<sup>1</sup>, Li Zong<sup>2</sup>, Yuru Kang<sup>2</sup> and Aiqin Wang<sup>2\*</sup>

<sup>1</sup>College of Chemistry and Chemical Engineering, Inner Mongolia University, Hohhot, China, <sup>2</sup>Key Laboratory of Clay Mineral Applied Research of Gansu Province, Lanzhou Institute of Chemical Physics, Chinese Academy of Sciences, Lanzhou, China

## OPEN ACCESS

### Edited by:

Marc Pera-Titus,  
Fudan University, China

### Reviewed by:

Chuanyi Wang,  
Shaanxi University of Science and  
Technology, China  
Amit Kumar Sharma,  
Indian Institute of Technology Mandi,  
India

### \*Correspondence:

Wenbo Wang  
boywenbo@126.com  
Aiqin Wang  
aqwang@licp.cas.cn

### Specialty section:

This article was submitted to  
Green and Sustainable Chemistry,  
a section of the journal  
Frontiers in Chemistry

**Received:** 01 February 2021

**Accepted:** 19 July 2021

**Published:** 28 July 2021

### Citation:

Wang W, Liu X, Wang X, Zong L,  
Kang Y and Wang A (2021) Fast and  
Highly Efficient Adsorption Removal of  
Toxic Pb(II) by a Reusable Porous  
Semi-IPN Hydrogel Based on Alginate  
and Poly(Vinyl Alcohol).  
Front. Chem. 9:662482.  
doi: 10.3389/fchem.2021.662482

A porous semi-interpenetrating network (semi-IPN) hydrogel adsorbent with excellent adsorption properties and removal efficiency towards Pb(II) was prepared by a facile grafting polymerization reaction in aqueous medium using natural biopolymer sodium alginate (SA) as the main chains, sodium acrylate (NaA) as the monomers, and poly(vinyl alcohol) (PVA) as the semi-IPN component. FTIR, TGA and SEM analyses confirm that NaA monomers were grafted onto the macromolecular chains of SA, and PVA chains were interpenetrated and entangled with the crosslinked network. The incorporation of PVA facilitates to form pores on the surface of hydrogel adsorbent. The semi-IPN hydrogel containing 2 wt% of PVA exhibits high adsorption capacity and fast adsorption rate for Pb(II). The best adsorption capacity reaches 784.97 mg/g, and the optimal removal rate reaches 98.39% (adsorbent dosage, 2 g/L). In addition, the incorporation of PVA improved the gel strength of hydrogel, and the storage modulus of hydrogel increased by 19.4% after incorporating 2 wt% of PVA. The increase of gel strength facilitates to improve the reusability of hydrogel. After 5 times of regeneration, the adsorption capacity of SA-g-PNaA decreased by 23.2%, while the adsorption capacity of semi-IPN hydrogel only decreased by 10.8%. The adsorption kinetics of the hydrogel in the initial stage (the moment when the adsorbent contacts solution) and the second stage are fitted by segmentation. It is intriguing that the adsorption kinetics fits well with both pseudo-second-order kinetic model and pseudo-first-order model before 60 s, while only fits well with pseudo-second-order adsorption model in the whole adsorption process. The chemical complexing adsorption mainly contribute to the efficient capturing of Pb(II).

**Keywords:** alginate, hydrogel, poly(vinyl alcohol), adsorption, lead(II)

## INTRODUCTION

In recent years, the rapid development of lead-zinc metallurgy, electroplating, batteries and other industries has discharged a large amount of toxic Pb(II)-containing wastewater, and the resulting water pollution problems become more and more serious, threatening people's health, survival and development. Presently, a variety of innovative technique has been developed and employed to decontaminate the harmful Pb(II) ions from polluted water (Vakili et al., 2019; Wang et al., 2019; Hoang et al., 2020). Among them, adsorption is commonly recognized as a potential method to

remove various pollutants (Au, 2020; Dong et al., 2020; Tamas et al., 2020). Using adsorption materials to remove heavy metal pollutants in water through physical or chemical action is considered to be one of the effective ways to eliminate Pb(II) pollution (Ezeokonkwo et al., 2018; Hashem et al., 2020). The design and development of new adsorbents with high adsorption capacity and fast adsorption rate have received considerable attention in both academic and industrial domains.

Hydrogel is a special polymer material with a moderately cross-linked network structure, which contains abundant functional groups in its unique network (Gull et al., 2020). The functional groups in the hydrogel's three-dimensional network will adsorb metal ions into the network through hydrogen bonds, electrostatic force and chemical complex interaction, and the network space will accommodate these adsorbed ions, so as to achieve high-capacity adsorption. Therefore, hydrogel adsorbents with higher adsorption capacity, faster adsorption rate and excellent desorption-regeneration ability are commonly regarded as highly efficient adsorbents. With the increasing attention on the environmental friendliness of materials, people are more inclined to use natural polymers to synthesize hydrogel materials for various purposes, because natural polymers have the advantages of being renewable, cheap, non-toxic and environmentally friendly (Wang et al., 2017; Kaur et al., 2020).

Sodium alginate (SA) is a water-soluble anionic biopolymer extracted from natural seaweed or produced by bacteria. Its structure is composed of  $\alpha$ -1, 4-L-glucuronic acid (G unit) and poly- $\beta$ -1, 4-D-mannuronic acid (M unit) with different ratios of 1–4. Because SA has the advantages of being renewable, abundant, safe, non-toxic, and biodegradable, it can be modified by ionic complex cross-linking, graft polymerization and chemical cross-linking reactions, so as to obtain new products with better performance (Yadav et al., 2011; Yadav and Rhee, 2012). In addition to the environmental friendliness of SA, the carboxyl groups on its molecular chain can serve as an active site for adsorbing metal ions, and the reactive -OH group on its molecular chain can also be easily modified by grafting reaction to obtain hydrogel materials with more functional groups (Wang and Wang, 2010). Due to the superior performance and eco-friendly advantages of SA, it has been widely used to prepare various polymer packing films (Saravanakumar et al., 2020; Zhang et al., 2020), drug-delivery vehicles (Mishra et al., 2021), antibacterial materials (Dwivedi et al., 2020), carrier of catalyst (Khan et al., 2020), superabsorbent hydrogel (Kassem et al., 2020), coatings (Fang et al., 2021) and adsorbent (Wang et al., 2013a; Gao et al., 2020). These materials derived from SA not only show excellent performance, but also exhibit unique eco-friendly advantages. Therefore, the SA-based polymer materials have received increasing attention for the decontamination of various pollutants from polluted water. The current focus is on improving the gel strength, regeneration capability and adsorption performance by introducing functional groups *via* grafting polymerization reaction or other functional components.

Semi-interpenetrating polymer network (semi-IPN) hydrogel is a polymer material with a structure similar to an "alloy", which

is composed of a chemically cross-linked polymer network and a linear polymer chain penetrating the polymer network. Due to the simultaneous presence of chemical crosslinking and physical crosslinking in this type of hydrogel, it has mechanical strength better than traditional hydrogels (Myung et al., 2008; Wang et al., 2013; Zhang et al., 2015). Polyvinyl alcohol (PVA) is a widely used non-toxic, biodegradable, water-soluble linear polymer, which has the inherent advantages of preparing ideal "green" materials (Yang et al., 2011). The polymer material prepared with PVA is not only non-toxic, but also has good biocompatibility, good viscoelasticity, strength and processability (Sahoo et al., 2002; Huang et al., 2012). PVA hydrogels have been used potentially in biomedicine and packaging, such as wound dressings (Kim, 2008), artificial articular cartilages (Kobayashi and Oka, 2004), drug delivery (Ossipov et al., 2013), and antibacterial material (Rafiq et al., 2018). PVA hydrogels can be prepared through physical or chemical crosslinking approach, and can also blend with other polymer chains to form composite gels. The neat chemically crosslinked hydrogel usually shows poor flexibility because the polymer chains were locked by chemical crosslinking points, which can't effectively transfer stress when the hydrogel being stretched (Liu et al., 2015). As a result, the hydrogel is brittle at swelling state, and is easily to be broken. It has been proven that PVA can form physical crosslinking with other polymer chains by non-covalent bonding interaction, which can effectively transfer stress when it was stretched or compressed by external forces. Therefore, incorporating PVA polymer chains into the cross-linked polymer network can improve the regularity of the network and increase the strength, hydrophilicity and other functional properties of the hydrogel network (Dragan, 2014). In light of the excellent advantages of SA and PVA, the semi-IPN hydrogel with improved gel strength and adsorption performance will be formed by combination of SA-g-PNaA and PVA *via* grafting polymerization reaction in water medium.

Based on the background mentioned above, the sodium alginate-g-poly(sodium acrylate)/poly(vinyl alcohol) (SA-g-PNaA/PVA) semi-IPN hydrogels was designed and synthesized in aqueous solution by free-radical grafting polymerization and crosslinking reactions. The as-prepared hydrogels were characterized by thermogravimetric analysis (TGA), Fourier transform infrared spectra (FTIR), and scanning electronic microscope (SEM). In addition, the role of PVA on improving the adsorption capacity for Pb(II), the gel strength and regeneration ability of the hydrogel was studied. The adsorption isotherm of the hydrogels towards Pb(II) were evaluated systematically. The adsorption kinetics and adsorption mechanism was explored.

## EXPERIMENTAL

### Materials

Sodium alginate (SA) (kinetic viscosity of 1.0 wt% aqueous solution, 20 cp), *N*, *N'*-methylene-*bis*-acrylamide (MBA, AR grade) and PbCl<sub>2</sub> (AR grade) was purchased from Sinopharm Chemical Reagent Co., Ltd., Shanghai, China. Acrylic acid (AA) and ammonium persulfate (APS, AR grade) were supplied by

Shanghai Regent Corp., Shanghai, China. PVA (Molecular weight, 85,000–124,000; alcoholysis degree is 95.5–96.5%) was purchased from Acros and used as received. All the other reagents used in this experiment are of analytical grade. All the chemicals used for this study were used as received. All the aqueous solutions are prepared with deionized water.

## Synthesis of SA-g-PNaA/PVA Hydrogels

At a temperature of 95°C, 30 ml of water and a predetermined amount of PVA (accounting for 2, 5, 10, 15, and 20% of the total mass of monomer AA and SA) were added in a four-necked flask equipped with a mechanical stirrer, a nitrogen tube, and a reflux condenser, and the mixture was stirred well to dissolve PVA to obtain a transparent solution. After the solution was cooled to 60°C, 1.0 g of SA powder was added thereto, and the mixture was continuously stirred until a uniform aqueous solution was formed. Then, under the protection of nitrogen, 10 ml of the aqueous solution containing 0.12 g of initiator APS was added, and the reactants were kept at 60°C for 10 min to decompose the initiator to generate free radicals. Immediately afterwards, a mixed solution containing 7.2 g acrylic acid (AA), 8 ml 8.0 mol/L NaOH solution and 72 mg cross-linking agent MBA was added to the flask under stirring, and the temperature was slowly raised to 70°C and kept at this temperature for 3 h to complete the polymerization reaction. After freezing the obtained hydrogel sample at –20°C, it was immersed in absolute ethanol for dehydration, and finally a dried product was obtained. The dried hydrogel was crushed and passed through a 100 mesh sieve for further use. According to a similar method, without adding PVA, the control sample SA-g-PNaA hydrogel was prepared. According to the amount of PVA, the SA-g-PNaA/PVA hydrogels are labeled as Semi-IPN2, Semi-IPN5, Semi-IPN10 and Semi-IPN20, respectively.

## Measurement of Gel Strength

The gel strength of hydrogel was tested by a previously reported rheological method, specifically the storage modulus and loss modulus of the hydrogel in the swollen state (water content controlled at 98%) was determined using a Physica MCR 301 rheometer (Germany) at 25° (Ramazani-Harandi et al., 2006). A parallel plate with the diameter of 25 mm was used to determine storage modulus ( $G'$ ). The deformation strain was fixed at 0.5%, and the angular frequency ( $\omega$ , rad/s) was fixed at 10 rad/s. The averages of three test results were reported in this paper.

## Evaluation of Adsorption Performance

The following procedures were employed to test the adsorption performance of the hydrogel adsorbent. Typically, 50 mg of the adsorbent was mixed with 25 ml of the aqueous solutions of Pb(II). Then, the mixture was shaken in a constant temperature shaker (THZ-98A, Yiheng, Shanghai, China) at a speed of 120 rpm and at 30°C for 120 min to make the adsorbent reach adsorption equilibrium. The solid adsorbent was rapidly separated from the aqueous Pb(II) solution by using a 0.22  $\mu\text{m}$  film filter. The concentration of Pb(II) ions in the filtered solution was determined with an atomic absorption spectrometry (Z-8000

AAS, Hitachi, Japan). The adsorption amount of Pb(II) onto unit mass of hydrogel adsorbent was calculated by the Eq. 1.

$$q = (C_0 - C_e)V/m \quad (1)$$

Here,  $q$  represents the adsorption amount of Pb(II) on the adsorbent at time  $t$  (marked as  $q_t$ ) or at equilibrium state (marked as  $q_e$ ), and its unit is “mg/g”;  $C_0$  and  $C_e$  represent the concentration of Pb(II) ions before and after adsorption, and its unit is “mg/L”;  $V$  represents the volume of Pb(II) solution after adsorption, and its unit is “L”;  $m$  represents the mass of the hydrogel adsorbent used for adsorption, and its unit is “g”.

In this work, the adsorption isotherm of the adsorbent for Pb(II) was tested in the initial concentration range of 880–3,200 mg/L (pH 5). Under the condition of the initial Pb(II) solution concentration of 1,150 mg/L, the adsorption performance of the adsorbent under different pH values (2.0–5.0) was tested, and the effect of pH on the adsorption behavior was studied. The pH value of the solution is adjusted with 0.1 mol/L HCl aqueous solution or NaOH solution. Use Eq. 1 to calculate the adsorption capacity of the hydrogel adsorbent. All adsorption experiments were performed 6 times in parallel, and the average of the data obtained was used for analysis and discussion. In order to investigate the adsorption isotherm of the hydrogel adsorbent and reveal how does the adsorbent interact with Pb(II) ions, the adsorption experiment data was fitted with Langmuir (Eq. 2) (Langmuir, 1916) and Freundlich (Eq. 3) (Freundlich, 1906) adsorption isotherm models.

$$C_e/q_e = 1/q_m b + C_e/q_m \quad (2)$$

$$\log q_e = \log K + (1/n)\log C_e \quad (3)$$

In these equations,  $q_e$  denotes the adsorption capacities of the adsorbents towards Pb(II) at equilibrium state, and its unit is “mg/g”;  $C_e$  denotes the residual concentration of Pb(II) solutions after being adsorbed with the hydrogel adsorbent, and its unit is “mg/L”.  $q_m$  refers to the saturated adsorption capacity of the hydrogel adsorbent, and its unit is “mg/g”.  $b$  is the Langmuir adsorption constant (L/mg) related to the free energy of adsorption.  $K$  (L/g) and  $n$  (dimensionless) represent Freundlich isotherm constant and heterogeneity factor, respectively.

The kinetic adsorption properties were tested according to the following procedure. Mixing 25 ml of Pb(II) solution (concentration is 1,150 mg/L) and 50 mg of adsorbent thoroughly, and then the mixture was filtered through a 0.22  $\mu\text{m}$  membrane filter at different time intervals (10–3,600 s) to make the solid adsorbent and the solution separate. The concentration of residual Pb(II) in the filtrate was determined by atomic absorption spectrometry and the adsorption capacities of the hydrogel adsorbent at each time interval were calculated according to Eq. 1. In order to study the adsorption kinetic of the adsorbent, the adsorption experimental data were fitted with pseudo-first-order model (Eq. 4) (Ho, 2004) and pseudo-second-order model (Eq. 5) (Ho and McKay, 1998), respectively.

$$\log(q_e - q_t) = \log q_e - (k_1/2.303)t \quad (4)$$

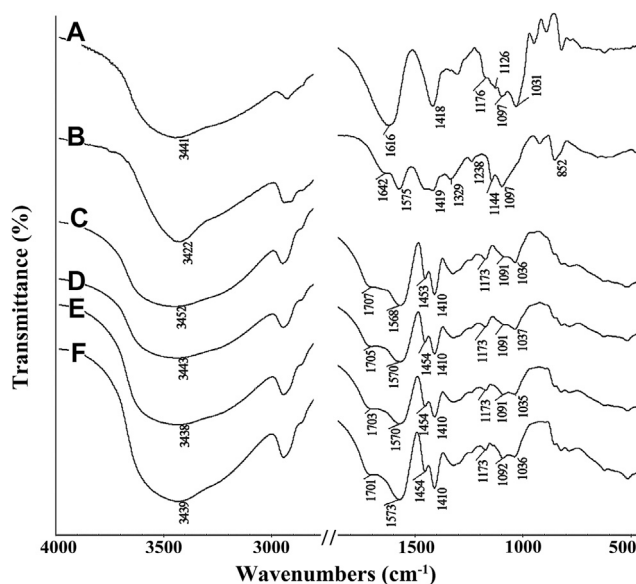


FIGURE 1 | FTIR spectra of (A) SA, (B) PVA, (C) Semi-IPN2, (D) Semi-IPN5, (E) Semi-IPN10, (F) Semi-IPN20.

$$t/q_t = 1/K_2 \times qe^2 + t/qe \quad (5)$$

In the two equations,  $q_e$  and  $q_t$  denote the adsorption amount of Pb(II) on unit mass of adsorbent at the equilibrium adsorption state and the adsorption time  $t$ , respectively, and their units are “mg/g.”  $k_1$  and  $k_2$  respectively refer to the rate constants obtained by fitting the pseudo-first-order kinetic model and the pseudo-second-order kinetic model.

## Measurement of Desorption and Regeneration Properties

Disperse 50 mg of adsorbents (SA-g-PNaA, Semi-IPN2 and Semi-IPN10, respectively) into 25 ml of Pb(II) solution (initial concentration is 1,150 mg/L, pH is 5) to reach equilibrium adsorption state. The adsorbent after adsorbing Pb(II) is filtered out, and re-dispersed in 25 ml of HNO<sub>3</sub> aqueous solution (0.1 mol/L) under magnetic stirring. After that, the adsorbent was separated from the aqueous solution by centrifugation. The obtained adsorbent was regenerated with 0.5 mol/L NaOH aqueous solution, followed by washing with deionized water 3 times, and then dried in an oven at 70°C and used for the next adsorption cycle. Atomic absorption spectrometry was used to determine the content of Pb(II) in the desorption solution to calculate the recovery rate. The adsorption and desorption treatment was carried out 5 times in succession, and the adsorption capacity of the adsorbent and recovery rate of Pb(II) with different regeneration times were obtained.

## Characterizations

A Thermo Nicolet NEXUS TM spectrophotometer was used to collect the FTIR spectra in the wavenumber region of 4,000–400 cm<sup>-1</sup>. The sample for test was uniformly mixed

with KBr by a gentle grinding process, and then pressed into disc-shaped KBr platelet. A field emission scanning electron microscope (FE-SEM, JSM-6701F, JEOL, Ltd., Japan) was employed to observe the morphologies of samples. Before observation, the sample was coated with gold film to enhance the conductivity of sample. The concentration of Pb(II) in the lixivium of the composites was determined by a Z-8000 AAS atomic absorption spectrophotometer (Hitachi, Japan). Thermogravimetric analysis (TGA) was performed on the Diamond TG-DTA 6300 thermal analyzer, the test temperature is 30~800°C, the gas atmosphere is N<sub>2</sub>, and the heating rate is 10°C/min.

## RESULTS AND DISCUSSION

### FTIR Spectra Analysis

The FTIR spectra of SA, PVA, SA-g-PNaA and the SA-g-PNaA/PVA hydrogels with different amounts of PVA are shown in **Figure 1**. The absorption peaks of SA at 1,616 cm<sup>-1</sup>, 1,418 cm<sup>-1</sup>, 1,176 cm<sup>-1</sup>, and 1,097 cm<sup>-1</sup> were ascribed to the O-C=O asymmetric stretching vibration, the O-C=O symmetric stretching vibration, the stretching vibration of C-O-C and the C-OH stretching vibration, respectively (**Figure 1A**) (Khalid et al., 2018). After the polymerization reaction, the new absorption peak at 1,707 cm<sup>-1</sup> (the C=O stretching vibration of -COOH groups) were observed in the FTIR spectra of the SA-g-PNaA/PVA hydrogel adsorbent (**Figures 1C-F**), and the C-OH stretching vibration peak of SA at 1,031 cm<sup>-1</sup> significantly weakened and shifted to 1,035–1,037 cm<sup>-1</sup>, indicating the C-OH groups of SA participate in grafting polymerization reaction, and the PNaA chains were grafted onto the SA molecular chains (Wang et al., 2013a). The characteristic absorption peaks of PVA were observed at 1,642 cm<sup>-1</sup> (C=O

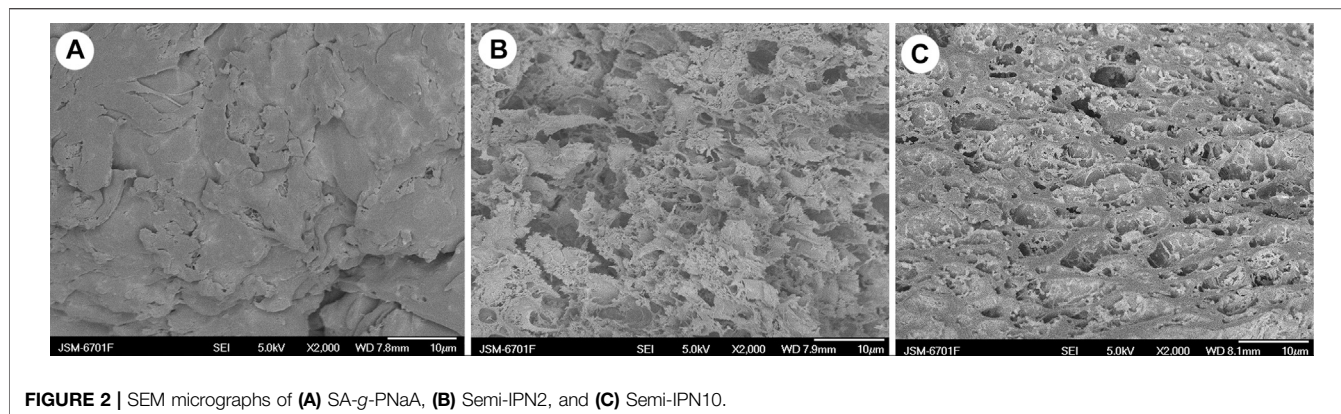


**FIGURE 2** | SEM micrographs of (A) SA-g-PNaA, (B) Semi-IPN2, and (C) Semi-IPN10.

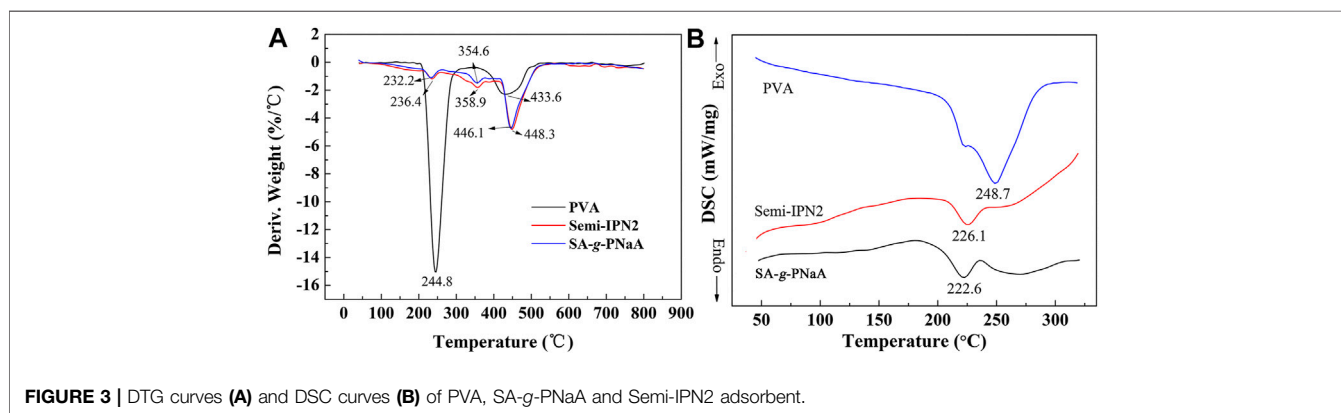


**FIGURE 3** | DTG curves (A) and DSC curves (B) of PVA, SA-g-PNaA and Semi-IPN2 adsorbent.

stretching of ester groups),  $1,419\text{ cm}^{-1}$  ( $-\text{OH}$  deformation),  $1,144\text{ cm}^{-1}$  (C-O-C stretching vibration), and  $1,097\text{ cm}^{-1}$  (C-OH stretching vibration) (Mansur et al., 2004). After polymerization reaction, the absorption peaks of PVA at  $1,144\text{ cm}^{-1}$  and  $1,097\text{ cm}^{-1}$  shift to  $1,091\text{ cm}^{-1}$  and  $1,036\text{ cm}^{-1}$  (also ascribed to the overlapping of the peak of PVA at  $1,097\text{ cm}^{-1}$  and the peak of SA at  $1,031\text{ cm}^{-1}$ ), respectively. In addition, the C=O stretching vibration peak of PVA at  $1,575\text{ cm}^{-1}$  shifted to  $1,568\text{--}1,573\text{ cm}^{-1}$  after grafting polymerization (Figures 1B–F). The above results indicate that hydrogen bond interaction occurs between PVA chains and the SA-g-PNaA polymer network (Dong et al., 2006; Sun and Uyama, 2013).

## Morphological Analysis

As is shown in Figure 2, the SA-g-PNaA hydrogel shows a dense surface with little wrinkles, pores and gaps (Figure 2A). However, loose surface and numerous pores were observed in the SEM micrographs of the Semi-IPN2 and Semi-IPN10 hydrogels (Figures 2B,C), indicating the incorporation of PVA is favorable to the formation of porous structure. For chemically crosslinked SA-g-PNaA hydrogel, the polymer chains were fixed by covalent crosslinking point, so the flexibility of gel network is poor, which may strongly shrink when it was dried to form a relatively dense surface. After incorporation of PVA, the flexibility of gel was improved, so the drying process does not induce the great change of network voids. After water was

removed, the three-dimensional network still remains well, and thus the macroporous hydrogel was obtained.

## DTG and DSC Analysis

The DTG diagrams of PVA, Semi-IPN2 and SA-g-PNaA are shown in Figure 3A. It can be seen from the DTG curve that the  $T_d$  (decomposition temperature corresponding to the maximum mass loss rate) values of PVA, Semi-IPN2 and SA-g-PNaA appear at  $244.8^\circ\text{C}$ ,  $446.1^\circ\text{C}$ , and  $448.3^\circ\text{C}$ , respectively. This indicates that the incorporation of PVA into the SA-g-PNaA network facilitates to improve its thermal stability because the  $-\text{OH}$  groups on PVA may form strong hydrogen bonding interaction or physical crosslinking points with the polymer chains in SA-g-PNaA network, which may limit the movement of linear polymer chain when it was heated. With the increase of PVA content, the  $T_d$  value also increased, due to the intensified interaction between PVA and the polymer matrix. After incorporation of 2 wt% PVA, the thermal decomposition temperature (centered at  $232.2^\circ\text{C}$ ) of SA-g-PNaA at the first stage on DTG curves increased to  $236.4^\circ\text{C}$ , and the thermal decomposition temperature (centered at  $354.6^\circ\text{C}$ ) of SA-g-PNaA at the second stage on DTG curves increased to  $358.9^\circ\text{C}$ , indicating that the incorporation of PVA improve the thermal stability of the Semi-IPN hydrogel by intensifying the interaction among polymer chains.

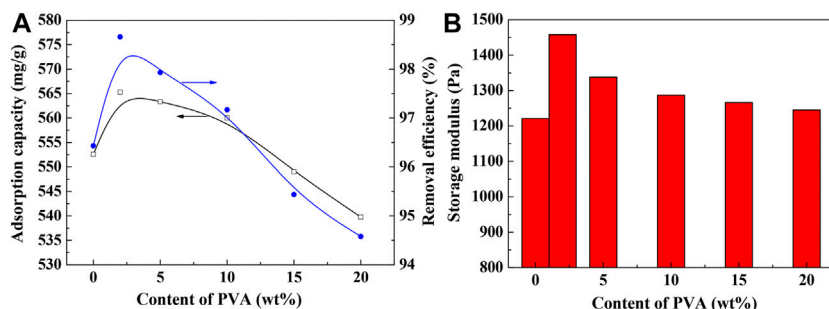


**FIGURE 4** | Effect of PVA content on the adsorption capacity (A) and the gel strength (B). Adsorption conditions: initial Pb(II) concentration, 1,150 mg/L; adsorbent dosage, 2 g/L; adsorption time, 120 min; pH, 5.0; adsorption temperature, 30°C.

As seen from **Figure 3B**, an endothermic peak at 248.7°C (ascribed to the dissociation process of hydrogen bonds among chains) was observed on the DSC curve of PVA. The endothermic peak of SA-g-PNaA appears at 222.6°C. When the PVA was incorporated into the crosslinked SA-g-PNaA network to form semi-IPN SA-g-PNaA/PVA hydrogel, the endothermic peak increased to 226.1°C (for Semi-IPN2). The increase of endothermic peak means the dissociation process of hydrogen bonds becomes difficult, and implied that the stronger tangle action between PVA chains and SA-g-PNaA network (Kulkarni et al., 2010).

## Effect of PVA Content on the Adsorption Capability and Gel Strength

The introduction of PVA containing large amounts of hydroxyl groups into the SA-g-PNaA hydrogel network may affect the network formulation of the hydrogel, and thus affect its adsorption capacity and gel strength. As shown in **Figure 4A**, the adsorption capacity and removal efficiency of the adsorbents towards Pb(II) initially increased with increasing the content of PVA to 2 wt%, and then decreased with the further increase of PVA content. The adsorption capacities of SA-g-PNaA and Semi-IPN2 toward Pb(II) are 554.53 mg/g and 568.99 mg/g, respectively, and the corresponding removal ratio of Pb(II) is 97.12 and 98.39% (initial Pb(II) concentration, 1,150 mg/L; pH 5), respectively.

As shown in **Figure 4B**, the incorporation of PVA has also contributed to improve the gel strength of the hydrogel adsorbents at wet state. The gel strength of the hydrogel increased by 19.4% after incorporation of 2 wt% of PVA. The increase of gel strength can be ascribed to the enhancement of the interaction among PVA chains and the grafting polymer chains (Li et al., 2018). PVA chains containing numerous -OH groups and -C=O groups was interpenetrated within the polymer network, which may form hydrogen bonding interaction with the -COO<sup>-</sup>, -OH, and -COOH groups in the SA-g-PNaA network and tangled with the grafted polymer chains to generate a physical crosslinking domain. The additional physical crosslinking is favorable to improve the viscoelasticity of the hydrogel, and thus enhance the gel strength of hydrogel (Pita-López et al., 2021). The increase of gel strength may improve the

stability of network structure, and enhance the adsorption capacity and reusability of the hydrogel adsorbent.

## Analysis of Adsorption Isotherms

**Figure 5** shows the dependence of adsorption capacity on the initial Pb(II) concentration and the curves fitting with Langmuir model. It is obvious that the adsorption capacity increased with increase of initial Pb(II) concentration, until equilibrium adsorption was attained at the initial concentrations of 3,200 mg/L. This is because as the concentration of Pb(II) ion in the external solution increases, a larger concentration gradient is generated between the bulk solution and the adsorbent, which makes the Pb(II) in the solution diffuse to the adsorbent and combine with the adsorbent more easily, so the adsorption capacity also increases (Xiong et al., 2010). On the contrary, as the initial Pb(II) concentration increases, the total amount of Pb(II) in the solution will also increase, and the removal rate of Pb(II) from the solution decreases. When the amount of Pb(II) adsorbed by the adsorbent is less than the amount of Pb(II) increased in the solution, the removal ratio will decrease. It is essential to interpret the adsorption behavior and predict the extent of adsorption by fitting the equilibrium adsorption data with Langmuir (Eq. 2) model, and Freundlich model (Eq. 3). As shown in **Figure 5B**, the plots of  $C_e/q_e$  vs.  $C_e$  exhibits perfect straight plots with  $R^2 > 0.9997$ . The parameters listed in **Table 1** can be obtained by fitting adsorption data to the Langmuir (plotting  $C_e/q_e$  vs.  $C_e$ ) and Freundlich (plotting  $\log q_e$  vs.  $\log C_e$ ) adsorption isotherm models. It was noticed from **Table 1** that the adsorption capacity calculated by fitting with Freundlich isotherm model ( $R^2 < 0.9447$ ) displays obvious difference with the experimental value; whereas the adsorption capacity obtained by fitting with Langmuir adsorption isotherm model ( $R^2 > 0.9997$ ) is close to the experimental value. This indicates that the adsorption process of the adsorbent for Pb(II) is in good agreement with the Langmuir isotherm model, and that Pb(II) is adsorbed onto the adsorbent through a single layer covering. The saturation adsorption capacities of Semi-IPN2 and Semi-IPN10 are determined to be 784.97 mg/g and 726.66 mg/g, respectively, which are better than most of other adsorbents (**Table 2**).

## Adsorption Kinetics

An ideal adsorption rate is the basic prerequisite to ensure the practical performance of the adsorbent. The type and number of

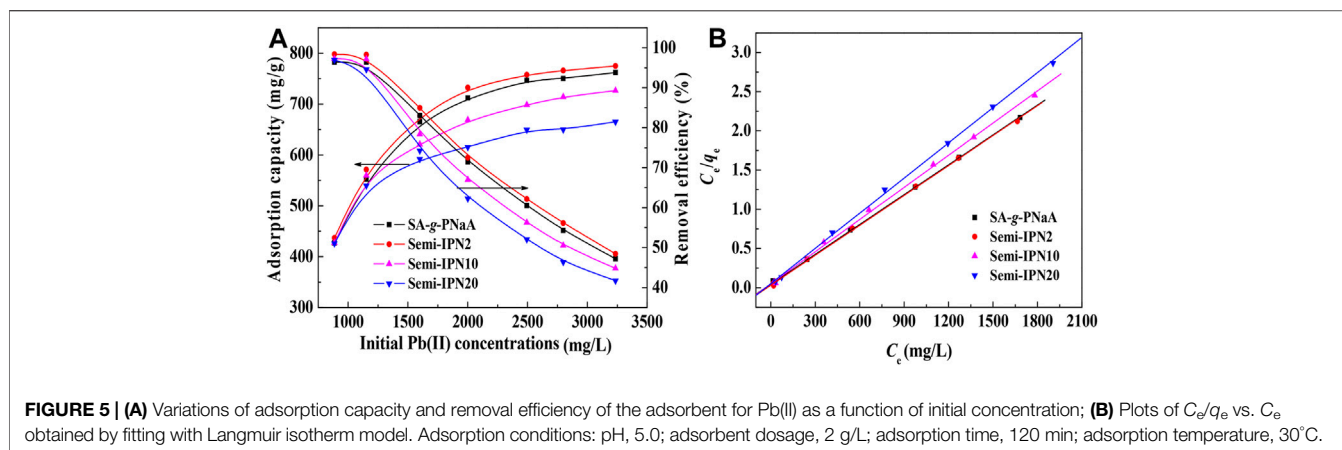


**TABLE 1 |** Adsorption isotherm parameters for the adsorption of Pb(II) ions onto the hydrogel adsorbent.

Samples	$q_e$ (mg/g)	Langmuir equation			Freundlich equation		
		$q_m$ (mg/g)	$b$ (L/mg)	$R^2$	$K$	$n$	$R^2$
SA-g-PNaA	775.92	781.25	0.0460	0.9998	368.03	9.558	0.9479
Semi-IPN2	784.97	787.40	0.0434	0.9997	372.88	9.708	0.9414
Semi-IPN10	726.66	729.93	0.0307	0.9996	351.61	10.189	0.9338
Semi-IPN20	665.05	666.67	0.0299	0.9997	328.22	10.487	0.9513

**TABLE 2 |** Comparison of the adsorption capacities of different adsorbents for Pb(II).

Adsorbents	Adsorption conditions	$q_e$ (mg/g)	Ref.
Polyacrylic acid grafted magnetic chitosan	Initial concentration, 500 mg/L; adsorbent dosage, 0.5 g/L; pH 5.48	204.89	Hu et al. (2020)
Spherical mesoporous silica	Initial concentration, 120 mg/L; adsorbent dosage, 1 g/L; pH 4	59.03	Zhu et al. (2016)
Hierarchical MgFe <sub>2</sub> O <sub>4</sub> microspheres	Initial concentration, 250 mg/L; adsorbent dosage, 0.5 g/L; pH 7	113.70	Kang et al. (2015)
Halloysite/alginate nanocomposite beads	Initial concentration, 200 mg/L; pH 5	325.00	Chiew et al. (2016)
Hydroxyapatite/chitosan porous materials	Initial concentration, 400 mg/L; pH 5.5	264.42	Lei et al. (2015)
CS coated cotton fiber	Initial concentration, 2,072 mg/L; pH 6.5	101.53	Zhang et al. (2008)
Amine functionalized rice husk magnetic nanoparticle biocomposites	Initial concentration, 350 mg/L; pH 5	680.19	Nata et al. (2020)
Alginate acid (AmAA)	Initial concentration, 800 mg/L; pH = 5, adsorbent dose = 0.25 g/L; time = 30 min	535.87	Vaid et al. (2020)
Semi-IPN2	Initial concentration, 1,150 mg/L; adsorbent dosage, 2 g/L; pH 5	568.99	This work
Semi-IPN2	Initial concentration, 3,200 mg/L; adsorbent dosage, 2 g/L; pH 5	784.97	This work

functional groups, pore structure and polymer network structure are the main factors affecting the adsorption rate of hydrogel materials. As shown in **Figure 6A**, in the initial stage, the adsorption capacity of Pb(II) by the adsorbent increases rapidly, and then the adsorption rate gradually slowed until the equilibrium adsorption was reached within 10 min. Comparatively, the semi-IPN hydrogel adsorbent has relatively rapid adsorption rate than the SA-g-PNaA hydrogel due to its relatively better porous structure. In order to study the adsorption kinetics of the adsorbent, the adsorption kinetic models of the pseudo-second-order (Eq. 4) and pseudo-first-order (Eq. 5) were used to fit the experimentally measured adsorption data. **Figure 6B** gives the fitting curves of the

hydrogel adsorbents using pseudo-second-order kinetic model. It was noticed that the fitting result at the shorter time ( $t \leq 50$  s) is not a perfect straight line (**Figure 6C**), but the fitting curve at the time larger than 120 s exhibits a perfect line ( $R^2 = 1.0000$ ) (**Figure 6F**). This indicates that the adsorption process of the hydrogel at the later part strictly follows the pseudo-second-order kinetic model very well. However, the linear correlation of the curve obtained by fitting the adsorption data at this stage with pseudo-first-order kinetic model is very poor (**Figure 6D**). Interestingly, the fitting curve of  $\log(q_e - q_t)$  versus  $t$  ( $\leq 50$  s) with pseudo-first-order kinetic model give the perfect straight line with the  $R^2$  values of 0.9988 and 0.9990 for SA-g-PNaA and Semi-IPN2, respectively (**Figure 6E**; **Table 3**), but a

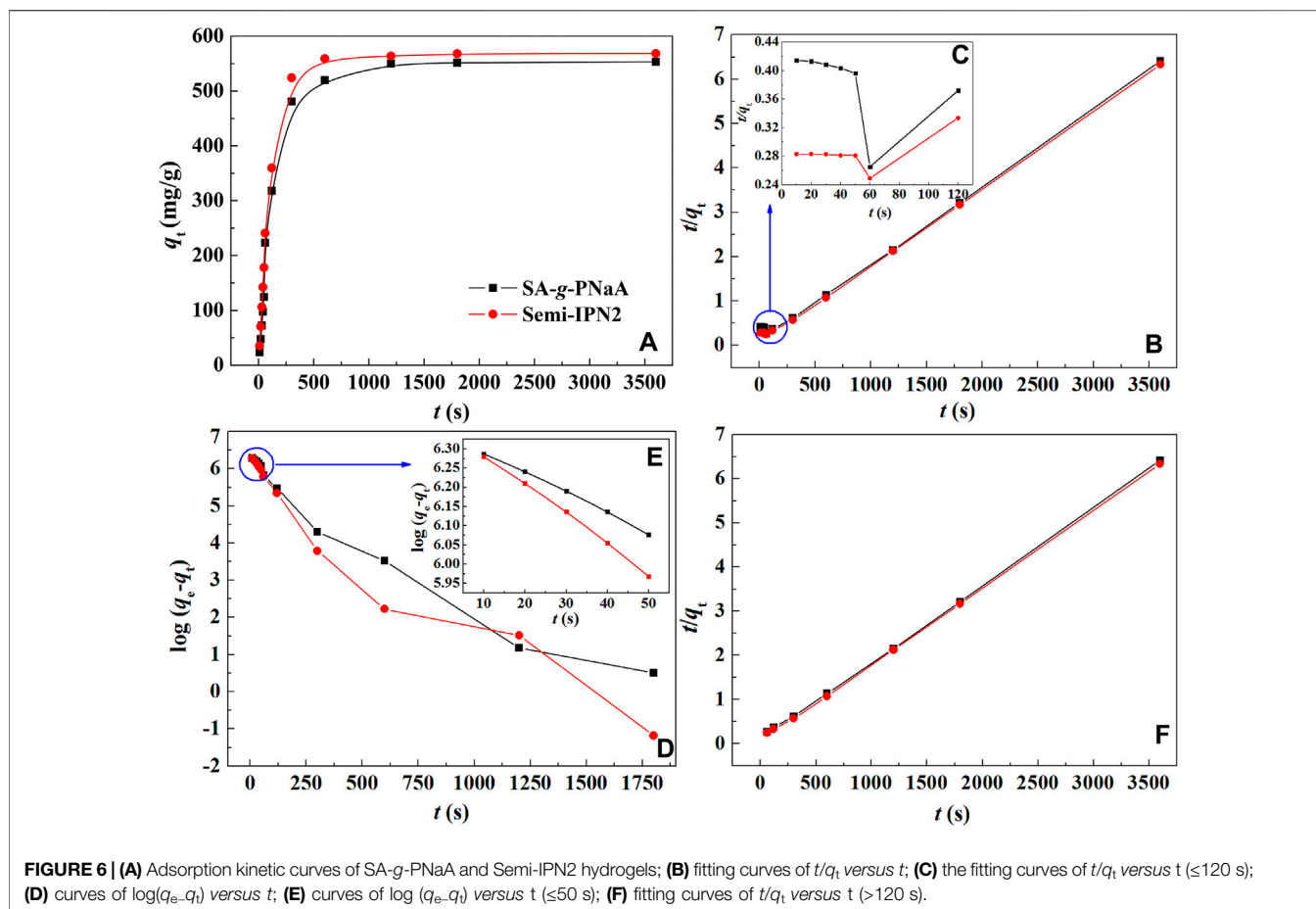


**TABLE 3 |** Adsorption kinetic parameters for adsorption of Pb(II) on the hydrogel.

Samples	Pseudo-first-order model				Pseudo-second-order model			
	$q_{e, \text{exp}}$ mg/g	$q_{m, \text{cal}}$ mg/g	$K_1$ $s^{-1}$	$R^2$	$q_{m, \text{cal}}$ mg/g	$k_2 \times 10^5$ g/(mg·s)	$k_{2i}$ mg/(g·s)	$R^2$
SA-g-PNaA	553.57	418.14	0.0080	0.9721	595.24	1.116	3.953	0.9981
Semi-IPN2	568.99	383.82	0.0095	0.9685	591.72	1.699	5.947	0.9991
$t \leq 50$ s, for Pseudo-first-order model					$t \geq 60$ s, for Pseudo-second-order model			
SA-g-PNaA	553.57	568.75	0.0121	0.9988	574.71	2.609	8.616	0.9998
Semi-IPN2	568.99	580.04	0.0179	0.9990	579.04	2.582	8.627	1.0000

poor line correlation with the  $R^2$  value  $< 0.9721$  was obtained for the whole adsorption process (Figure 6D; Table 3). It can be noticed that the  $q_{e, \text{cal}}$  value calculated with pseudo-second-order model ( $t \geq 60$  s) is close to that calculated with the pseudo-first-order model ( $t \leq 50$  s), and these values are more close to the experimental values. The results show that when the adsorption time  $t \leq 50$  s, the kinetic behavior of the adsorbent to adsorb Pb(II) obeys both the pseudo-first-order kinetic model and the pseudo-second-order kinetic model. During the initial adsorption process, the physical diffusion adsorption and chemical adsorption contribute to Pb(II) adsorption. As a whole, the physical diffusion adsorption is dominant at initial stage ( $t \leq 50$  s) and

chemical adsorption is dominant at the following stage ( $t \geq 60$  s), and the inflection point of these two processes appears at 60 s.

As shown in Table 3, the adsorption rate constant of the SA-g-PNaA hydrogel is  $0.0121 \text{ s}^{-1}$  at initial stage, but increased to  $0.0179 \text{ s}^{-1}$  for Semi-IPN2. The pseudo-second-order kinetic constant of SA-g-PNaA is  $3.953 \text{ mg/g}\cdot\text{s}$ , but increased to  $5.947 \text{ mg/g}\cdot\text{s}$  for Semi-IPN2. These results indicate that the introduction of PVA may clearly increase the adsorption rate of the hydrogel, which is favorable to the practical application of hydrogel. The main reason may be that the PVA improved the network structure of the hydrogel, and make the network becomes regular. In addition, the incorporation of PVA can

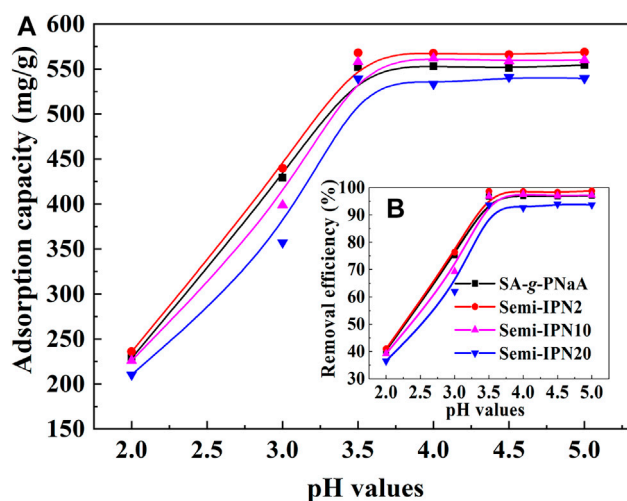


**FIGURE 7** | Variable curves of adsorption capacity (A) and removal efficiency (B) against the change of pH values.

improve the porous morphology of the as-prepared hydrogel, which can reduce the transport resistance of metal ions in the polymer network, thereby increasing the adsorption rate.

## pH-Responsive Adsorption Behavior and Mechanisms

The main reason why the hydrogel adsorbent can efficiently adsorb Pb(II) ions is the complexation of the functional groups in the network structure to Pb(II) and the electrostatic attraction of the network structure to Pb(II) ions. The change of external pH values may affect the existence stage of functional groups and thus affect the adsorption behaviors. As is shown in **Figure 7**, the adsorption capacity and removal efficiency of the hydrogel adsorbents for Pb(II) sharply increased with increasing the external pH values, and almost keep constant at pH above 3.5. The maximum adsorption capacity of the Semi-IPN2 adsorbent sample at pH 5 is 568.99 mg/g (**Figure 7**), and the corresponding removal rate is 98.39%. The main reasons can be ascribed to the transformation between  $\text{-COOH}$  and  $\text{-COO}^-$  groups. The pKa value of poly(acrylic acid) is about 4.7 (Chen et al., 2008), so the  $\text{-COO}^-$  groups on the hydrogel adsorbent were transformed as  $\text{-COOH}$  groups at acidic pH (<3.5). The  $\text{-COOH}$  groups may form strong hydrogen bonds with the functional groups in the hydrogel network to form additional crosslinking, and thus the network shrinks and its capture capability to metal ions decreased. Also, the  $\text{-COOH}$  groups have relatively weaker complexing ability to Pb(II) ions than  $\text{-COO}^-$  groups, so the increase of  $\text{-COO}^-$  amounts causes the increase of adsorption capacity (Astrini et al., 2015). In addition, the increase of the negative charge on the surface of the adsorbent with increasing pH is also one of the reasons for the enhancement of adsorption capacity. At pH 2, the Zeta potential of the adsorbent is +2.6 mV. When the pH value increases to 3.5 and 5, the Zeta potential is  $-9.6$  mV, and  $-20.21$  mV, respectively. As the pH of the solution increases, the Zeta potential of the adsorbent becomes more negative. This is conducive to the adsorbent's ability to efficiently adsorb positively charged metal ions.

In order to explore the adsorption mechanism, the FTIR spectra of the Semi-IPN2 hydrogel adsorbent after Pb(II) adsorption under different pH conditions were analyzed. As shown in **Figure 8**, after adsorbing Pb(II) at different pH values, the characteristic absorption peak of the adsorbent changed significantly. The characteristic bands of the adsorbent appear at  $1707\text{ cm}^{-1}$  (C = o stretching vibration of  $\text{-COOH}$  groups),  $1568\text{ cm}^{-1}$  (asymmetric stretching vibration of  $\text{-COO}^-$  groups),  $1453\text{ cm}^{-1}$  and  $1410\text{ cm}^{-1}$  (symmetrical stretching vibration of  $\text{-COO}^-$  groups),  $1091\text{ cm}^{-1}$  (C-O-C stretching vibration),  $1036\text{ cm}^{-1}$  (C-OH stretching vibration). After adsorption of Pb(II) at pH 3, 3.5, 4, 4.5, and 5, the C=O absorption bands of  $\text{-COOH}$  groups in the adsorbent shift from  $1707\text{ cm}^{-1}$  to  $1716$  and  $1639\text{ cm}^{-1}$ ,  $1707\text{ cm}^{-1}$ ,  $1704\text{ cm}^{-1}$ ,  $1703\text{ cm}^{-1}$ , and  $1703\text{ cm}^{-1}$ , respectively; the bands of  $\text{-COO}^-$  groups at  $1568\text{ cm}^{-1}$  shift to  $1540\text{ cm}^{-1}$ ,  $1538\text{ cm}^{-1}$ ,  $1526\text{ cm}^{-1}$ ,  $1525\text{ cm}^{-1}$ , and  $1523\text{ cm}^{-1}$ , respectively. The shift of the C = o stretching vibration of  $\text{-COOH}$  groups to  $1638\text{ cm}^{-1}$  (**Figure 8A**) and  $1635\text{ cm}^{-1}$  (**Figure 8B**) after adsorption of Pb(II) at pH 3 and 3.5 indicates that the part of  $\text{-COOH}$  was complexed with the Pb(II), and another part was still present in the form of  $\text{-COOH}$  (Zhu et al., 2015). The shift of the asymmetric stretching vibration peak of  $\text{-COO}^-$  groups from  $1568\text{ cm}^{-1}$  to  $1540\text{ cm}^{-1}$  indicates most of the  $\text{-COO}^-$  groups were complexed with Pb(II) ions (**Figure 8B**). When the pH values are higher than 3.5, the shift of the characteristic peaks of the  $\text{-COO}^-$  groups becomes more obvious, which shifted to  $1526\text{ cm}^{-1}$ ,  $1525\text{ cm}^{-1}$ , and  $1523\text{ cm}^{-1}$  after adsorption of Pb(II) at pH 4, 4.5, and 5, respectively (**Figures 8C-E**). At the same time, the symmetrical stretching vibration peak of  $\text{-COO}^-$  groups also shifts obviously. The obvious shift of adsorption peak proves that the  $\text{-COO}^-$  groups chelates with Pb(II) to form a stable chemical bonding interaction. These results indicate that the stronger chemical complexing action between  $\text{-COO}^-$  groups and Pb(II) mainly contribute to the efficient adsorption of adsorbent towards Pb(II) (Wang et al., 2009) (**Scheme 1**). The conventional pore adsorption, electrostatic attraction and ion-exchange also have

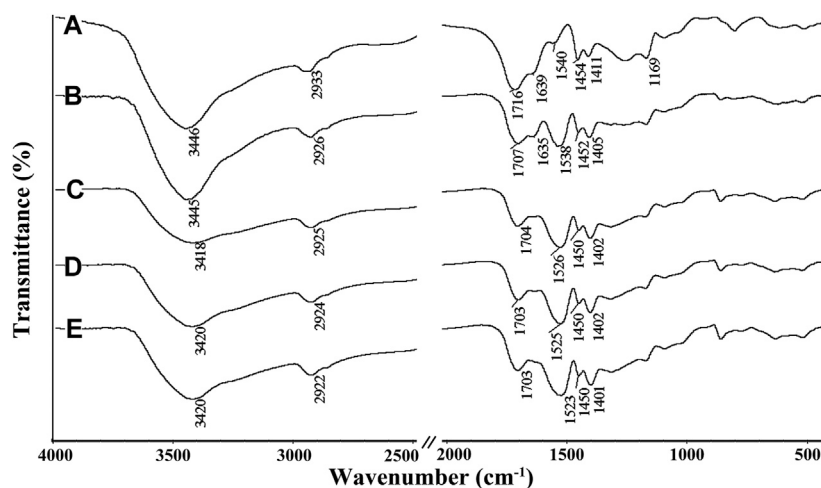
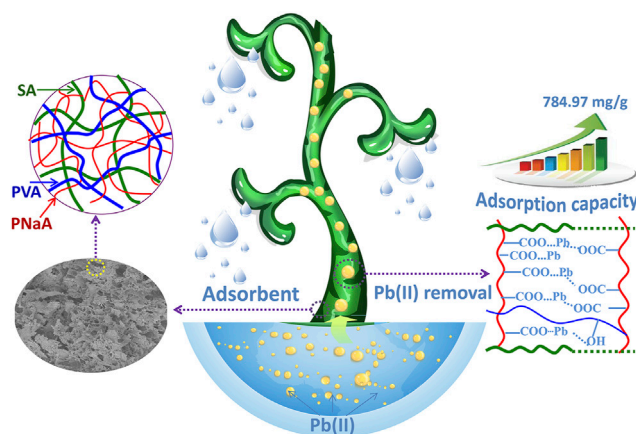


**FIGURE 8** | FTIR spectra of Semi-IPN2 adsorbent after adsorption of Pb(II) at the pH values of (A) 3, (B) 3.5, (C) 4, (D) 4.5, and (E) 5.



**SCHEME 1** | Scheme illustrated the gel network structure of the adsorbent and its adsorption actions for Pb(II).

contribution to the adsorption process, but chemical complexing is the dominant driving forces.

## Desorption of Pb(II) and the Regeneration of Adsorbent

An excellent adsorbent usually needs to have excellent regeneration performance and reusability, and it is desired to have the ability to adsorb heavy metals and desorb/recover metal ions at the same time. Regeneration can reduce the use cost of adsorbents, and the recovery of metal ions can reduce the waste of valuable metal resources. With dilute  $\text{HNO}_3$  aqueous solution, the adsorbed metal ions can be quickly and easily desorbed, and the metal ions can be converted into soluble nitrate for reuse at the same time. As shown in **Figure 9**, the adsorption capacity slightly decreased with increasing the usage times, but the adsorption capacity to Pb(II) still reach 502.5 mg/g (for Semi-IPN2) after reused for 5 cycles, which is obviously higher than that of SA-g-PNaA (427.2 mg/g), indicating that the Semi-IPN2

hydrogel adsorbent has relatively better regeneration capability than SA-g-PNaA hydrogel. It can be calculated from the desorption data that about 93.6% of the Pb(II) adsorbed by the semi-IPN2 adsorbent can be de-adsorbed and recycled by acid-leaching process, and about 89.9% of the Pb(II) adsorbed by the reused adsorbent (regenerated for 5 times) can be de-adsorbed and recycled. In general, the direct use or reuse of environmentally friendly biopolymer-based hydrogel adsorption materials can simultaneously achieve the purification of heavy metal polluted wastewater, the enrichment of metal ions and the recycling of metal ions, which have great potential as water treatment and separation materials.

## CONCLUSIONS

The porous semi-IPN hydrogel adsorbent SA-g-PNaA/PVA with very fast adsorption rate and superior adsorption capability towards Pb(II) were prepared by a one-pot

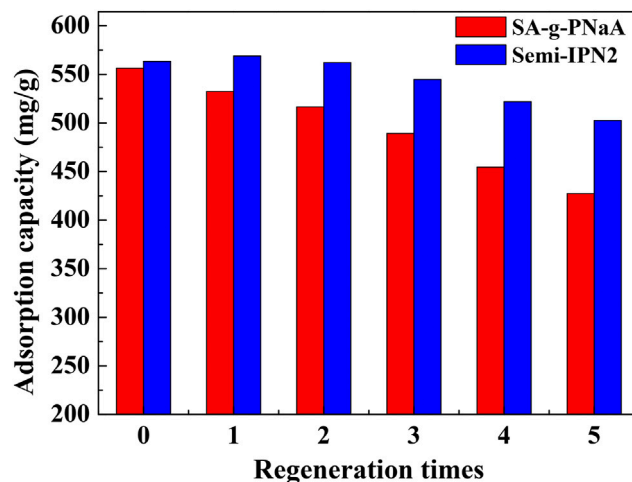


**FIGURE 9** | The adsorption capacity of the SA-g-PNaA and Semi-IPN2 adsorbents towards Pb(II) after adsorption-desorption for 5 cycles.

polymerization reaction in water medium using PVA as the interpenetrating polymer components. Incorporating 2 wt% of PVA not only improved the adsorption capacity of the hydrogel adsorbent, but also enhanced the gel strength of hydrogel by 119%. The maximum saturation adsorption capacity reaches 784.97 mg/g for the optimal Semi-IPN2 adsorbent, and a high removal ratio of 98.39% was reached at the adsorbent dosage of 2 g/L (initial Pb(II) concentration, 1,150 mg/L). About 93.60% of the adsorbed Pb(II) can be easily desorbed with HNO<sub>3</sub> and recycled. Incorporating PVA also improved the reusability of hydrogel adsorbent for adsorption of Pb(II), and the Semi-IPN2 adsorbent can still reach the adsorption capacity of 502.5 mg/g toward Pb(II) after regenerated and reused for 5 cycles, which is significantly better than the SA-g-PNaA adsorbent. The adsorption kinetic curves fits well with pseudo-first-order kinetic equation at initial stage ( $t \leq 50$  s), which revealed a physical diffusion adsorption process at this stage. However, the adsorption data can be fitted well with pseudo-second-order kinetic equation at second stage ( $t > 60$  s) with the best  $R^2$  value of 1.0000, which reveal that chemical adsorption process is dominant at this stage. The chemical complex and electrostatic attraction between -COO<sup>-</sup> and Pb(II) are the main driving forces for the high adsorption capacity and fast adsorption rate of the hydrogel, and ion exchange also assists the adsorption process. This paper provides a method for preparing a new type of biopolymer-based environmentally friendly high-efficiency adsorbent. The obtained adsorbent can be used to

adsorb and recover Pb(II) from a high-concentration solution, which can be used potentially for high-efficiency purification of heavy metal polluted water and enrichment of metal ion.

## DATA AVAILABILITY STATEMENT

The original contributions presented in the study are included in the article/supplementary material, further inquiries can be directed to the corresponding authors.

## AUTHOR CONTRIBUTIONS

WW and XL contribute to the design of experiment, the experiment process and data analysis; wrote the paper and drawn all the figures. XW contributes to the experiment process and data analysis. LZ and YK contribute to the structure characterization and revision of the paper. AW contributes to the experiment design, data analysis, and revision of the paper.

## FUNDING

The Scientific Research start-up funding from Inner Mongolia University (21300-5205122) and National Natural Science Foundation of China (21706267 and 51403221).

## REFERENCES

- Astrini, N., Anah, L., and Haryadi, H. R. (2015). Adsorption of Heavy Metal Ion from Aqueous Solution by Using Cellulose Based Hydrogel Composite. *Macromol. Symp.* 353, 191–197. doi:10.1002/masy.201550326
- Au, V. K.-M. (2020). Recent Advances in the Use of Metal-Organic Frameworks for Dye Adsorption. *Front. Chem.* 8, 708. doi:10.3389/fchem.2020.00708
- Chen, Y., Ding, D., Mao, Z., He, Y., Hu, Y., Wu, W., et al. (2008). Synthesis of Hydroxypropylcellulose-Poly(acrylic Acid) Particles with Semi-interpenetrating Polymer Network Structure. *Biomacromolecules* 9, 2609–2614. doi:10.1021/bm800484e
- Chiew, C. S. C., Yeoh, H. K., Pasbakhsh, P., Krishnaiah, K., Poh, P. E., Tey, B. T., et al. (2016). Halloysite/alginate Nanocomposite Beads: Kinetics, Equilibrium and Mechanism for lead Adsorption. *Appl. Clay Sci.* 119, 301–310. doi:10.1016/j.clay.2015.10.032

- Dong, W., Lu, Y., Wang, W., Zhang, M., Jing, Y., and Wang, A. (2020). A Sustainable Approach to Fabricate New 1D and 2D Nanomaterials from Natural Abundant Palygorskite clay for Antibacterial and Adsorption. *Chem. Eng. J.* 382, 122984. doi:10.1016/j.cej.2019.122984
- Dong, Y. Q., Zhang, L., Shen, J. N., Song, M. Y., and Chen, H. L. (2006). Preparation of Poly(vinyl Alcohol)-Sodium Alginate Hollow-Fiber Composite Membranes and Pervaporation Dehydration Characterization of Aqueous Alcohol Mixtures. *Desalination* 193, 202–210. doi:10.1016/j.desal.2005.08.023
- Dragan, E. S. (2014). Design and Applications of Interpenetrating Polymer Network Hydrogels. A Review. *Chem. Eng.* 243, 572–590. doi:10.1016/j.cej.2014.01.065
- Dwivedi, L. M., Baranwal, K., Gupta, S., Mishra, M., Sundaram, S., and Singh, V. (2020). Antibacterial Nanostructures Derived from Oxidized Sodium Alginate-ZnO. *Int. J. Biol. Macromolecules* 149, 1323–1330. doi:10.1016/j.jbiomac.2020.02.011
- Ezeokonkwo, M. A., Ofor, O. F., and Ani, J. U. (2018). Preparation and Evaluation of Adsorbents from Coal and Irvingia Gabonensis Seed Shell for the Removal of Cd(II) and Pb(II) Ions from Aqueous Solutions. *Front. Chem.* 5, 132. doi:10.3389/fchem.2017.00132
- Fang, H., Wang, C., Zhou, S., Li, G., Tian, Y., and Suga, T. (2021). Exploration of the Enhanced Performances for Silk Fibroin/sodium Alginate Composite Coatings on Biodegradable Mg–Zn–Ca alloy. *J. Magnesium Alloys.* doi:10.1016/j.jma.2020.08.017
- Freundlich, H. (1906). Over the Adsorption in Solution. *J. Phys. Chem.* 57, 1100–1107.
- Gao, X., Guo, C., Hao, J., Zhao, Z., Long, H., and Li, M. (2020). Adsorption of Heavy Metal Ions by Sodium Alginate Based Adsorbent-A Review and New Perspectives. *Int. J. Biol. Macromolecules* 164, 4423–4434. doi:10.1016/j.jbiomac.2020.09.046
- Gull, N., Khan, S. M., Khalid, S., Zia, S., Islam, A., Sabir, A., et al. (2020). Designing of Biocompatible and Biodegradable Chitosan Based Crosslinked Hydrogel for *In Vitro* Release of Encapsulated Povidone-Iodine: A Clinical Translation. *Int. J. Biol. Macromolecules* 164, 4370–4380. doi:10.1016/j.jbiomac.2020.09.031
- Hashem, A., Fletcher, A. J., Younis, H., Mauof, H., and Abou-Okeil, A. (2020). Adsorption of Pb(II) Ions from Contaminated Water by 1,2,3,4-butanetetracarboxylic Acid-Modified Microcrystalline Cellulose: Isotherms, Kinetics, and Thermodynamic Studies. *Int. J. Biol. Macromolecules* 164, 3193–3203. doi:10.1016/j.jbiomac.2020.08.159
- Ho, Y. S. (2004). A Review of Potentially Low Cost Adsorbent for Heavy Metals. *Scientometrics* 59, 171–177.
- Ho, Y. S., and McKay, G. (1998). A Comparison of Chemisorption Kinetic Models Applied to Pollutant Removal on Various Sorbents. *Process Saf. Environ. Prot.* 76, 332–340. doi:10.1205/095758298529696
- Hoang, M. T., Pham, T. D., Verheyen, D., Nguyen, M. K., Pham, T. T., Zhu, J., et al. (2020). Fabrication of Thin Film Nanocomposite Nanofiltration Membrane Incorporated with Cellulose Nanocrystals for Removal of Cu(II) and Pb(II). *Chem. Eng. Sci.* 228, 115998. doi:10.1016/j.ces.2020.115998
- Hu, D., Lian, Z., Xian, H., Jiang, R., Wang, N., Weng, Y., et al. (2020). Adsorption of Pb(II) from Aqueous Solution by Polyacrylic Acid Grafted Magnetic Chitosan Nanocomposite. *Int. J. Biol. Macromolecules* 154, 1537–1547. doi:10.1016/j.jbiomac.2019.11.038
- Huang, D., Wang, W., Xu, J., and Wang, A. (2012). Mechanical and Water Resistance Properties of Chitosan/poly(vinyl Alcohol) Films Reinforced with Attapulgite Dispersed by High-Pressure Homogenization. *Chem. Eng. J.* 210, 166–172. doi:10.1016/j.cej.2012.08.096
- Kang, D., Yu, X., Ge, M., and Song, W. (2015). One-step Fabrication and Characterization of Hierarchical MgFe<sub>2</sub>O<sub>4</sub> Microspheres and Their Application for lead Removal. *Microporous Mesoporous Mater.* 207, 170–178. doi:10.1016/j.micromeso.2015.01.023
- Kassem, I., Kassab, Z., Khoulood, M., Sehaqui, H., Bouhfid, R., Jacquemin, J., et al. (2020). Phosphoric Acid-Mediated green Preparation of Regenerated Cellulose Spheres and Their Use for All-Cellulose Cross-Linked Superabsorbent Hydrogels. *Int. J. Biol. Macromolecules* 162, 136–149. doi:10.1016/j.jbiomac.2020.06.136
- Kaur, A., Singh, D., and Sud, D. (2020). A Review on Grafted, Crosslinked and Composites of Biopolymer Xanthan Gum for Phasing Out Synthetic Dyes and Toxic Metal Ions from Aqueous Solutions. *J. Polym. Res.* 27, 297. doi:10.1007/s10965-020-02271-6
- Khalid, I., Ahmad, M., Minhas, M. U., and Barkat, K. (2018). Preparation and Characterization of Alginate-PVA-Based Semi-IPN: Controlled Release pH-Responsive Composites. *Polym. Bull.* 75, 1075–1099. doi:10.1007/s00289-017-2079-y
- Khan, S. B., Ahmad, S., Kamal, T., Asiri, A. M., and Bakhsh, E. M. (2020). Metal Nanoparticles Decorated Sodium Alginate-carbon N-itrile C-composite Beads as Effective Catalyst for the Reduction of Organic Pollutants. *Int. J. Biol. Macromolecules* 164, 1087–1098. doi:10.1016/j.jbiomac.2020.07.091
- Kobayashi, M., and Oka, M. (2004). Characterization of a Polyvinyl Alcohol-Hydrogel Artificial Articular Cartilage Prepared by Injection Molding. *J. Biomater. Sci. Polym. Edition* 15 (6), 741–751. doi:10.1163/156856204774196135
- Kim, S. W. (2008). Preparation and Barrier Property of Poly(Vinyl Alcohol)/SiO<sub>2</sub> Hybrid Coating Films. *Korean J. Chem. Eng.* 25, 1195–1200. doi:10.1007/s11814-008-0197-9
- Kulkarni, R. V., Sreedhar, V., Mutalik, S., Setty, C. M., and Sa, B. (2010). Interpenetrating Network Hydrogel Membranes of Sodium Alginate and Poly(vinyl Alcohol) for Controlled Release of Prazosin Hydrochloride through Skin. *Int. J. Biol. Macromolecules* 47, 520–527. doi:10.1016/j.jbiomac.2010.07.009
- Langmuir, I. (1916). The Constitution and Fundamental Properties of Solids and Liquids. Part I. Solids. *J. Am. Chem. Soc.* 38, 2221–2295. doi:10.1021/ja02268a002
- Lei, Y., Guan, J.-J., Chen, W., Ke, Q.-F., Zhang, C.-Q., and Guo, Y.-P. (2015). Fabrication of Hydroxyapatite/chitosan Porous Materials for Pb(II) Removal from Aqueous Solution. *RSC Adv.* 5 (32), 25462–25470. doi:10.1039/c5ra01628b
- Li, X., Shu, M., Li, H., Gao, X., Long, S., Hu, T., et al. (2018). Strong, Tough and Mechanically Self-Recoverable Poly(vinyl Alcohol)/alginate Dual-Physical Double-Network Hydrogels with Large Cross-Link Density Contrast. *RSC Adv.* 8, 16674–16689. doi:10.1039/c8ra01302k
- Liu, X. J., Ren, X. Y., Guan, S., Li, H. Q., Song, Z. K., and Gao, G. H. (2015). Highly Stretchable and Tough Double Network Hydrogels via Molecular Stent. *Eur. Polym. J.* 73, 149–161. doi:10.1016/j.eurpolymj.2015.10.011
- Mansur, H. S., Oréface, R. L., and Mansur, A. A. P. (2004). Characterization of Poly(vinyl Alcohol)/poly(ethylene Glycol) Hydrogels and PVA-Derived Hybrids by Small-Angle X-ray Scattering and FTIR Spectroscopy. *Polymer* 45 (21), 7193–7202. doi:10.1016/j.polymer.2004.08.036
- Mishra, A., Pandey, V. K., Shankar, B. S., and Melo, J. S. (2021). Spray Drying as an Efficient Route for Synthesis of Silica Nanoparticles-Sodium Alginate Biohybrid Drug Carrier of Doxorubicin. *Colloids Surf. B: Biointerfaces* 197, 111445. doi:10.1016/j.colsurfb.2020.111445
- Myung, D., Waters, D., Wiseman, M., Duhamel, P.-E., Noolandi, J., Ta, C. N., et al. (2008). Progress in the Development of Interpenetrating Polymer Network Hydrogels. *Polym. Adv. Technol.* 19, 647–657. doi:10.1002/pat.1134
- Nata, I. F., Wicakso, D. R., Mirwan, A., Irawan, C., Ramadhani, D., and Ursulla (2020). Selective Adsorption of Pb(II) Ion on Amine-Rich Functionalized rice Husk Magnetic Nanoparticle Biocomposites in Aqueous Solution. *J. Environ. Chem. Eng.* 8, 104339. doi:10.1016/j.jece.2020.104339
- Ossipov, D., Kootala, S., Yi, Z., Yang, X., and Hilborn, J. (2013). Orthogonal Chemoselective Assembly of Hyaluronic Acid Networks and Nanogels for Drug Delivery. *Macromolecules* 46 (10), 4105–4113. doi:10.1021/ma400543u
- Pita-López, M. L., Fletes-Vargas, G., Espinosa-Andrews, H., and Rodríguez-Rodríguez, R. (2021). Physically Cross-Linked Chitosan-Based Hydrogels for Tissue Engineering Applications: A State-Of-The-Art Review. *Eur. Polym. J.* 145, 110176. doi:10.1016/j.eurpolymj.2020.110176
- Rafiq, M., Hussain, T., Abid, S., Nazir, A., and Masood, R. (2018). Development of Sodium Alginate/PVA Antibacterial Nanofibers by the Incorporation of Essential Oils. *Mater. Res. Express* 5, 035007. doi:10.1088/2053-1591/aab0b4
- Ramazani-Harandi, M. J., Zohuriaan-Mehr, M. J., Yousefi, A. A., Ershad-Langroudi, A., and Kabiri, K. (2006). Rheological Determination of the Swollen Gel Strength of Superabsorbent Polymer Hydrogels. *Polym. Test.* 25, 470–474. doi:10.1016/j.polymertesting.2006.01.011
- Sahoo, S. K., Panyam, J., Prabha, S., and Labhasetwar, V. (2002). Residual Polyvinyl Alcohol Associated with Poly (D,L-lactide-co-glycolide) Nanoparticles Affects Their Physical Properties and Cellular Uptake. *J. Controlled Release* 82 (1), 105–114. doi:10.1016/s0168-3659(02)00127-x

- Saravanakumar, K., Sathiyaseelan, A., Mariadoss, A. V. A., Xiaowen, H., and Wang, M.-H. (2020). Physical and Bioactivities of Biopolymeric Films Incorporated with Cellulose, Sodium Alginate and Copper Oxide Nanoparticles for Food Packaging Application. *Int. J. Biol. Macromolecules* 153, 207–214. doi:10.1016/j.ijbiomac.2020.02.250
- Sun, X. X., and Uyama, H. (2013). A Poly(vinyl Alcohol)/sodium Alginate Blend Monolith with Nanoscale Porous Structure. *Nanoscale Res. Lett.* 8, 411. doi:10.1186/1556-276x-8-411
- Tămaș, A., Cozma, I., Cochei, L., Lupa, L., and Rusu, G. (2020). Adsorption of Orange II onto Zn<sub>2</sub>Al-Layered Double Hydroxide Prepared from Zinc Ash. *Front. Chem.* 8, 573535. doi:10.3389/fchem.2020.573535
- Vaid, U., Mittal, S., Babu, J. N., and Kumar, R. (2020). Amido-amine Derivative of Alginic Acid (AmaA) for Enhanced Adsorption of Pb(II) from Aqueous Solution. *Int. J. Biol. Macromolecules* 147, 499–512. doi:10.1016/j.ijbiomac.2020.01.040
- Vakili, M., Deng, S., Cagnetta, G., Wang, W., Meng, P., Liu, D., et al. (2019). Regeneration of Chitosan-Based Adsorbents Used in Heavy Metal Adsorption: A Review. *Separat. Purif. Technol.* 224, 373–387. doi:10.1016/j.seppur.2019.05.040
- Wang, F., Zhu, Y. F., Wang, W. B., Zong, L., Lu, T. T., and Wang, A. Q. (2017). Fabrication of CMC-G-PAM Superporous Polymer Monoliths via Eco-Friendly Pickering-MIPES for superior Adsorption of Methyl Violet and Methylene Blue. *Front. Chem.* 5, 33. doi:10.3389/fchem.2017.00033
- Wang, F., Zhu, Y. F., Xu, H., and Wang, A. Q. (2019). Preparation of Carboxymethyl Cellulose-Based Macroporous Adsorbent by Eco-Friendly Pickering-MIPES Template for Fast Removal of Pb<sup>2+</sup> and Cd<sup>2+</sup>. *Front. Chem.* 7, 603. doi:10.3389/fchem.2019.00603
- Wang, W., Zong, L., and Wang, A. (2013a). A Nanoporous Hydrogel Based on Vinyl-Functionalized Alginate for Efficient Adsorption and Removal of Pb<sup>2+</sup> Ions. *Int. J. Biol. Macromol.* 62, 225–231. doi:10.1016/j.ijbiomac.2013.08.038
- Wang, W., and Wang, A. (2010). Synthesis and Swelling Properties of pH-Sensitive Semi-IPN Superabsorbent Hydrogels Based on Sodium Alginate-G-Poly(sodium Acrylate) and Polyvinylpyrrolidone. *Carbohydr. Polym.* 80 (4), 1028–1036. doi:10.1016/j.carbpol.2010.01.020
- Wang, W.-B., Huang, D.-J., Kang, Y.-R., and Wang, A.-Q. (2013b). One-Step in Situ Fabrication of a Granular Semi-IPN Hydrogel Based on Chitosan and Gelatin for Fast and Efficient Adsorption of Cu<sup>2+</sup> ion. *Colloids Surf. B: Biointerfaces* 106, 51–59. doi:10.1016/j.colsurfb.2013.01.030
- Wang, X., Zheng, Y., and Wang, A. (2009). Fast Removal of Copper Ions from Aqueous Solution by Chitosan-G-Poly(acrylic Acid)/attapulgitite Composites. *J. Hazard. Mater.* 168, 970–977. doi:10.1016/j.jhazmat.2009.02.120
- Xiong, L., Yang, Y., Mai, J., Sun, W., Zhang, C., Wei, D., et al. (2010). Adsorption Behavior of Methylene Blue onto Titanate Nanotubes. *Chem. Eng. J.* 156, 313–320. doi:10.1016/j.cej.2009.10.023
- Yadav, M., Mishra, D. K., Sand, A., and Behari, K. (2011). Modification of Alginate through the Grafting of 2-acrylamidoglycolic Acid and Study of Physicochemical Properties in Terms of Swelling Capacity, Metal Ion Sorption, Flocculation and Biodegradability. *Carbohydr. Polym.* 84, 83–89. doi:10.1016/j.carbpol.2010.10.065
- Yadav, M., and Rhee, K. Y. (2012). Superabsorbent Nanocomposite (alginate-g-PAMPS/MMT): Synthesis, Characterization and Swelling Behavior. *Carbohydr. Polym.* 90, 165–173. doi:10.1016/j.carbpol.2012.05.010
- Yang, D., Yu, K., Ai, Y., Zhen, H., Nie, J., and Kennedy, J. F. (2011). The Mineralization of Electrospun Chitosan/poly(vinyl Alcohol) Nanofibrous Membranes. *Carbohydr. Polym.* 84 (3), 990–996. doi:10.1016/j.carbpol.2010.12.057
- Zhang, G., Qu, R., Sun, C., Ji, C., Chen, H., Wang, C., et al. (2008). Adsorption for Metal Ions of Chitosan Coated Cotton Fiber. *J. Appl. Polym. Sci.* 110, 2321–2327. doi:10.1002/app.27515
- Zhang, H., Pang, X., and Qi, Y. (2015). pH-Sensitive Graphene Oxide/sodium Alginate/polyacrylamide Nanocomposite Semi-IPN Hydrogel with Improved Mechanical Strength. *RSC Adv.* 5 (108), 89083–89091. doi:10.1039/c5ra19637j
- Zhang, H., Wang, W., Ding, J., Lu, Y., Xu, J., and Wang, A. (2020). An Upgraded and Universal Strategy to Reinforce Chitosan/polyvinylpyrrolidone Film by Incorporating Active Silica Nanorods Derived from Natural Palygorskite. *Int. J. Biol. Macromolecules* 165 (Part A), 1276–1285. doi:10.1016/j.ijbiomac.2020.09.241
- Zhu, W., Li, X., Wu, D., Yu, J., Zhou, Y., Luo, Y., et al. (2016). Synthesis of Spherical Mesoporous Silica Materials by Pseudomorphic Transformation of Silica Fume and its Pb<sup>2+</sup> Removal Properties. *Microporous Mesoporous Mater.* 222, 192–201. doi:10.1016/j.micromeso.2015.10.013
- Zhu, Y., Zheng, Y., Wang, W., and Wang, A. (2015). Highly Efficient Adsorption of Hg(II) and Pb(II) onto Chitosan-Based Granular Adsorbent Containing Thiourea Groups. *J. Water Process Eng.* 7, 218–226. doi:10.1016/j.jwpe.2015.06.010

**Conflict of Interest:** The authors declare that the research was conducted in the absence of any commercial or financial relationships that could be construed as a potential conflict of interest.

**Publisher's Note:** All claims expressed in this article are solely those of the authors and do not necessarily represent those of their affiliated organizations, or those of the publisher, the editors and the reviewers. Any product that may be evaluated in this article, or claim that may be made by its manufacturer, is not guaranteed or endorsed by the publisher.

Copyright © 2021 Wang, Liu, Wang, Zong, Kang and Wang. This is an open-access article distributed under the terms of the Creative Commons Attribution License (CC BY). The use, distribution or reproduction in other forums is permitted, provided the original author(s) and the copyright owner(s) are credited and that the original publication in this journal is cited, in accordance with accepted academic practice. No use, distribution or reproduction is permitted which does not comply with these terms.